aerospace

MDPI

Article

Statistical CSI-Based Downlink Precoding for Multi-Beam LEO Satellite Communications

Feng Zhu [1,*], Yunfei Wang [1], Ziyu Xiang [1,2] and Xiqi Gao [1,2]

[1] Purple Mountain Laboratories, Nanjing 211100, China; wangyunfei@pmlabs.com.cn (Y.W.); ziyuxiang@seu.edu.cn (Z.X.); xqgao@seu.edu.cn (X.G.)
[2] National Mobile Communications Research Laboratory, Southeast University, Nanjing 211100, China
* Correspondence: zhufeng@pmlabs.com.cn

Abstract

With the rapid development of low-Earth-orbit (LEO) satellite communications, multi-beam precoding has emerged as a key technology for improving spectrum efficiency. However, the long propagation delay and large Doppler frequency offset pose significant challenges to existing precoding techniques. To address this issue, this paper investigates downlink precoding design for multi-beam LEO satellite communications. First, the downlink channel and signal models are established. Then, we reveal that traditional zero-forcing (ZF), regularized zero-forcing (RZF), and minimum mean square error (MMSE) precoding schemes all require the satellite transmitter to acquire the instantaneous channel state information (iCSI) of all users, which is challenging to obtain in satellite communication systems. Subsequently, we propose a downlink precoding design based on statistical channel state information (sCSI) and derive closed-form solutions for statistical-ZF, statistical-RZF, and statistical-MMSE precoding. Furthermore, we propose that sCSI can be computed using the positions of the satellite and users, which reduces the system overhead and complexity of sCSI acquisition. Monte Carlo simulations under the 3GPP non-terrestrial network (NTN) channel model are employed to verify the performance of the proposed method. The simulation results show that the proposed method achieves sum-rate performance comparable to that of iCSI-based schemes and the optimal transmission performance based on sum-rate maximization. In addition, the proposed method significantly reduces the computational complexity of the satellite payload and the system feedback overhead.

Keywords: LEO satellite communication; multi-beam; precoding; sCSI

Check for updates

Academic Editor: M. Reza Emami

Received: 25 November 2025
Revised: 4 January 2026
Accepted: 6 January 2026
Published: 7 January 2026

Copyright: © 2026 by the authors. Licensee MDPI, Basel, Switzerland. This article is an open access article distributed under the terms and conditions of the Creative Commons Attribution (CC BY) license.

1. Introduction

Satellite communication is crucial for achieving global coverage, enabling convenient satellite network services for users worldwide [1–3]. The 3rd-generation partnership project (3GPP) introduced non-terrestrial network (NTN) technology in the 5th-generation new radio (5G NR) as a vital supplement to terrestrial cellular communication, and released the first NTN standard supporting satellite communication in 2022. Satellite communication is also explicitly included in the 6th-generation (6G) vision defined by the international telecommunication union (ITU) [4,5].

In recent years, constellations represented by Starlink and OneWeb have driven the development of low-Earth-orbit (LEO) mega-constellation networks, characterized by large scale, wide coverage, low latency, and high bandwidth capabilities [2]. With the rapid advancement of satellite communications, satellite direct-to-device (DTD) has gradually

emerged as a new focus in satellite communications, offering enormous industrial application prospects [6–8]. To support satellite DTD, satellites are typically equipped with large-scale phased array antennas (PAAs) to enhance antenna gain and meet the link requirements. Additionally, they operate in the sub-6 GHz frequency band to mitigate link loss.

Current satellite communication systems generally adopt a multi-beam architecture. However, co-channel interference between beams in multi-beam systems remains unavoidable. Existing multi-beam satellite communication systems typically employ a multi-color reuse scheme. Although this scheme can mitigate interference between adjacent beams, it is limited by low spectrum resource reuse capability. To further utilize limited spectrum resources, multi-beam satellite communication can adopt a full frequency reuse (FFR) scheme, where all beams use the same frequency band. Nevertheless, this also introduces more significant co-channel interference between beams and across satellites. Researchers have addressed the inter-beam interference caused by FFR among different beams in [9,10]. Given the ever-growing demand for high throughput, the FFR scheme and precoding technology are regarded as the most critical technologies. During the standardization process of 3GPP, many companies have proposed to further improve system throughput using multiple-input–multiple-output (MIMO) technology in Release 20 and future 6G NTN [11–14].

1.1. Related Work

Numerous investigations have been focused on multi-beam joint transmission techniques in satellite communication systems. For fixed multi-beam satellite systems, the design of joint multi-user linear precoding for the forward link was explored in [15], and an iterative algorithm that alternates between the optimization of precoding vectors and power allocation strategies was proposed therein. In the context of geostationary-Earth-orbit (GEO) multi-beam high-throughput satellite (HTS) communications, a user scheduling and power allocation approach based on regularized zero-forcing (RZF) precoding was put forward in [16]. A hopping beam design scheme grounded in minimum mean square error (MMSE) precoding was introduced in another study by [17]. Regarding low-Earth-orbit (LEO) satellite communications, hybrid analog–digital precoding has been the focus of research in [18,19]. Additionally, the joint optimization of beam directions alongside the allocation of spectrum, time, and power resources in dynamic multi-beam LEO satellite networks was examined in [20]; the proposed method is capable of enhancing the number of supported users and boosting system throughput. Nevertheless, all the aforementioned works, from [15–20], require that instantaneous channel state information (iCSI) be obtained by the satellite transmitter, a requirement that poses considerable challenges in practical satellite communication systems [21].

Imperfect channel state information (CSI) has been explored in several studies to enhance the robustness of transmission strategies in satellite communications. In the framework of FFR, a robust multi-group multicast beamforming design tailored for satellite downlinks was proposed in [22]. This design was based on a beam-domain channel model that incorporated the effects of channel phase uncertainty. Concurrently, robust multi-group multicast precoding techniques for frame-structured multi-beam satellite communication systems were delved into, and a user clustering approach relying on partial CSI was introduced in [23,24]. A zero-forcing (ZF) precoding scheme using partial CSI was further proposed in [25], though this scheme is limited to GEO HTS systems and solely utilizes antenna patterns and path loss information. While these methods all leverage imperfect CSI to improve the robustness of their transmission schemes, a key requirement remains that the transmitter must still acquire partial CSI. An energy-aware opportunistic routing strategy

to guarantee the maximum data transfer rate was proposed in [26]. A robust precoding method based on deep reinforcement learning, applicable to LEO satellites operating under imperfect CSI conditions, was investigated in [27]. A downlink precoding method based on sum-rate maximization was proposed in [28]. However, the designs in [27,28] necessitate iterative computations, which result in extremely high computational complexity.

In summary, as presented in Table 1, existing multi-beam satellite precoding research can be broadly categorized into iCSI-based and partial CSI-based approaches. iCSI-based schemes [15–20] acquire instantaneous channel state information through frequent feedback. However, the frequent channel estimation and feedback processes consume a substantial amount of limited system overhead, and the long round-trip transmission delay in satellite communications may exceed the channel coherence time, rendering the obtained iCSI outdated. Existing partial CSI-based precoding [22–28] still requires the transmitter to acquire partial channel state information. Moreover, these precoding designs lack closed-form solutions and require iterative computation, leading to extremely high computational complexity that is unsuitable for satellite payload implementation.

Table 1. Comparison of representative multi-beam precoding schemes.

Prior Work	CSI Type	Complexity	System Overhead	Weaknesses
Zheng [15]	iCSI	middle	high	difficult to acquire iCSI
Chien [16]	iCSI	middle	high	difficult to acquire iCSI
Chen [17]	iCSI	middle	high	difficult to acquire iCSI
Han [18]	iCSI	middle	high	difficult to acquire iCSI
Wang [19]	iCSI	middle	high	difficult to acquire iCSI
Yuan [20]	iCSI	high	high	difficult to acquire iCSI
You [22]	partial CSI	high	middle	still need to feedback partial CSI, high computational complexity
Wang [23]	partial CSI	high	middle	still need to feedback partial CSI, high computational complexity
Wang [24]	partial CSI	high	middle	still need to feedback partial CSI, high computational complexity
Ahmad [25]	imperfect CSI	middle	middle	GEO, not suitable for LEO.
Schröder [27]	imperfect CSI	high	middle	extremely high computational complexity.
Li [28]	partial CSI	high	high	extremely high computational complexity.

1.2. Motivations and Contributions

To bridge the above gap, this paper focuses on addressing two unresolved issues: first, designing a low-complexity precoding method with a closed-form expression to reduce computational complexity while achieving near-optimal transmission performance for multi-beam LEO satellite communications; second, significantly reducing the difficulty and system overhead associated with statistical channel state information (sCSI) acquisition. To this end, this paper investigates the downlink precoding design based on sCSI for multi-beam LEO satellite communications.

The major contributions are summarized as follows:

- We establish the downlink channel and signal transmission models for orthogonal frequency division multiplexing (OFDM)-based multi-beam LEO satellite communication systems.
- We propose to design downlink precoding using sCSI and derive closed-form solutions for statistical-zero-forcing (statistical-ZF), statistical-regularized zero-forcing (statistical-RZF), and statistical-minimum mean square error (statistical-MMSE) precoding. sCSI includes the array response vectors of each user on the satellite side and the average downlink channel power. Compared with iCSI, sCSI is substantially easier to acquire at the transmitter. Precoding vectors based on sCSI can be

computed over a longer sCSI update period, reducing the computational requirements for on-board processing.

- We propose a method to calculate sCSI using information such as satellite position and user position. Thus, users only need to periodically report their position information without estimating and feeding back CSI, which significantly reduces system overhead.
- We present numerical simulation results to demonstrate that the proposed method can substantially improve the system sum-rate performance.

1.3. Organization

The remainder of this paper is organized as follows. Section 2 introduces the system model, including the channel model, signal transmission model, and system architecture. Conventional iCSI-based precoding methods are presented in Section 3. In Section 4, the proposed sCSI-based precoding methods are detailed. Section 5 describes the sCSI acquisition method. Section 6 provides the simulation results and analysis. Finally, Section 7 concludes this paper.

2. System Model

This section establishes the downlink channel and signal transmission model for LEO satellite communications. First, the channel and signal models are derived for the OFDM-based multi-beam LEO satellite communication system. Second, the statistical characteristics of the downlink satellite channel are analyzed, which lays a theoretical foundation for the acquisition of sCSI in subsequent sections. Then, the system architecture of the downlink precoding scheme at the satellite transmitter is presented, along with the corresponding signal model for downlink precoding.

Consider an OFDM-based broadband multi-beam LEO satellite communication system. As shown in Figure 1, the satellite is equipped with a uniform planar array (UPA) antenna, where the number of antennas along the x-axis and y-axis is M_x and M_y, respectively, and the total number of antennas is $M = M_x \times M_y$. Each user is equipped with a single antenna. The satellite generates K downlink beams through a beamforming network (BFN) to serve K users simultaneously, with $K \ll M$.

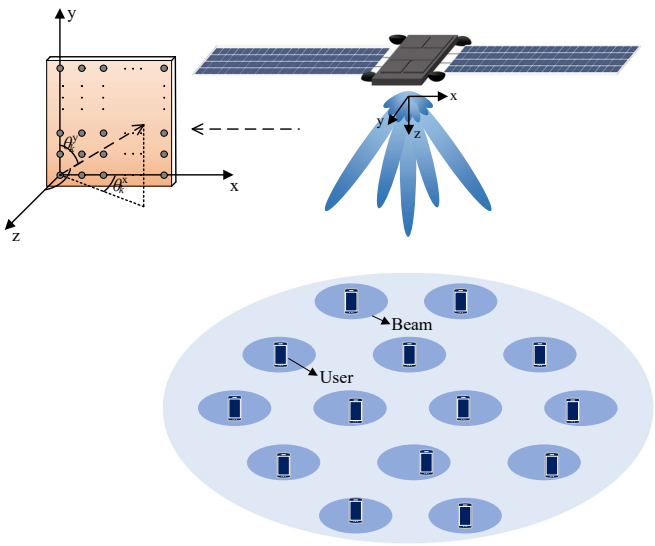


Figure 1. LEO satellite communication system.

For the downlink, the channel response between the satellite and user k can be expressed as

$$\breve{\mathbf{h}}_k^H(t,\tau) = \sum_{l=0}^{L_k-1} a_{k,l} e^{\bar{\jmath}2\pi\nu_{k,l}t}\delta(\tau-\tau_{k,l})\mathbf{g}_{k,l}^H, \tag{1}$$

where $\bar{\jmath}=\sqrt{-1}$, L_k represents the number of multipaths for user k, $a_{k,l}$ denotes the channel complex gain, $\nu_{k,l}$ is the Doppler shift, $\tau_{k,l}$ is the propagation delay, and $\mathbf{g}_{k,l}\in\mathbb{C}^{M\times 1}$ is the array response vector at the satellite. The Doppler shift $\nu_{k,l}$ is the sum of the large Doppler $\nu_{k,l}^{\text{sat}}$ caused by the high-speed movement of the satellite and the conventional Doppler $\nu_{k,l}^{\text{ut}}$ caused by the movement of the user. The propagation delay $\tau_{k,l}$ consists of the minimum satellite–ground propagation delay $\tau_k^{\min}=\min_l\tau_{k,l}$ and the multipath delay $\tau_{k,l}^{\text{ut}}$ on the user side. Since scatterers in satellite communication systems are distributed near users and there are no scatterers on the satellite side, the angular spread of the multipath arriving at the satellite is almost zero, and the angles of different paths at the satellite are similar [21,28]. Therefore, the channel on the satellite side exhibits a single-path characteristic, i.e., $\mathbf{g}_{k,l}=\mathbf{g}_k$, and $\mathbf{g}_k$ can be expressed as

$$\mathbf{g}_k = \mathbf{g}_k^{\text{x}}(\tilde{\theta}_k^{\text{x}})\otimes\mathbf{g}_k^{\text{y}}(\tilde{\theta}_k^{\text{y}}), \tag{2}$$

where $\tilde{\theta}_k^{\text{x}}$ and $\tilde{\theta}_k^{\text{y}}$ denote the directional cosines of user k with respect to the x-axis and y-axis, respectively, which reflect the space domain property of the channel for user k. $\tilde{\theta}_k^{\text{x}}$ and $\tilde{\theta}_k^{\text{y}}$ are given by

$$\tilde{\theta}_k^{\text{x}} = \sin\theta_k^{\text{y}}\cos\theta_k^{\text{x}}, \tag{3a}$$

$$\tilde{\theta}_k^{\text{y}} = \cos\theta_k^{\text{y}}, \tag{3b}$$

where θ_k^{x} and θ_k^{y} represent the angles of departure (AoDs) of user k. $\mathbf{g}_k^{\text{v}}(\tilde{\theta}_k^{\text{v}})\in\mathbb{C}^{M_{\text{v}}\times 1}$ can be written as

$$\mathbf{g}_k^{\text{v}}(\tilde{\theta}_k^{\text{v}}) = \frac{1}{\sqrt{M_{\text{v}}}}\left(1, e^{-\bar{\jmath}\frac{2\pi d_{\text{v}}}{\lambda}\tilde{\theta}_k^{\text{v}}}, \cdots, e^{-\bar{\jmath}\frac{2\pi d_{\text{v}}}{\lambda}(M_{\text{v}}-1)\tilde{\theta}_k^{\text{v}}}\right)^T, \tag{4}$$

where λ is the downlink carrier wavelength, and M_{v} and d_{v} denote the number of antenna elements and the adjacent antenna distance along the v-axis with $\text{v}\in\{\text{x},\text{y}\}$ at the satellite, respectively.

Let N_{sc}, N_{cp}, and T_{s} be the number of subcarriers, the length of the cyclic prefix (CP), and the sampling period, respectively. Then, the CP duration is $T_{\text{cp}}=N_{\text{cp}}T_{\text{s}}$ and the time duration of the OFDM symbol including CP is $T=T_{\text{sc}}+T_{\text{cp}}$, where $T_{\text{cp}}=N_{\text{cp}}T_{\text{s}}$ is the time duration of the CP and $T_{\text{sc}}=N_{\text{sc}}T_{\text{s}}$ is the time duration of the OFDM symbol excluding the CP.

Defining $x_{k,s,r}, r=0,1,\cdots,N_{\text{sc}}-1$ as the downlink transmitted symbol over the r-th subcarrier at the s-th OFDM symbol for user k, the transmitted symbol in the time domain can be written as

$$x_{k,s}(t) = \sum_{r=0}^{N_{\text{sc}}-1} x_{k,s,r}e^{\bar{\jmath}2\pi r\Delta f t}, \quad -T_{\text{cp}}\le t-sT\le T_{\text{sc}}, \tag{5}$$

where $\Delta f=1/T_{\text{sc}}$. Let $\mathbf{b}_k\in\mathbb{C}^{M\times 1}$ be the downlink beamforming vector for user k, which satisfies $||\mathbf{b}_k||=1$. The downlink transmitted symbol can be denoted as

$$\mathbf{x}_s(t) = \sum_{i=1}^{K}\mathbf{b}_i x_{i,s}. \tag{6}$$

Then, the downlink received signal at user k can be expressed as

$$y_{k,s}(t) = \int_{-\infty}^{\infty} \breve{\mathbf{h}}_k^H(t,\tau)\mathbf{x}_s(t-\tau)\mathrm{d}\tau + z_{k,s}(t), \tag{7}$$

where $z_{k,s}(t)$ denotes the additive white Gaussian noise (AWGN) of the user k within the s-th OFDM symbol.

After performing Doppler and delay compensation on the user side, the compensated downlink time-domain received signal is given by

$$\begin{aligned} y_{k,s}^{\mathrm{cps}}(t) &= y_{k,s}(t+\tau_k^{\mathrm{cps}})e^{-\bar{\jmath}2\pi\nu_k^{\mathrm{cps}}(t+\tau_k^{\mathrm{cps}})} \\ &= \int_{-\infty}^{\infty} \tilde{\mathbf{h}}_k^H(t,\tau)\mathbf{x}_s(t-\tau)\mathrm{d}\tau + z_{k,s}(t), \end{aligned} \tag{8}$$

where $\tilde{\mathbf{h}}_k^H(t,\tau)$ denotes the downlink equivalent impulse response of user k after Doppler shift and delay compensation, which can be expressed as

$$\tilde{\mathbf{h}}_k^H(t,\tau) = \sum_{l=0}^{L_k-1} \tilde{a}_{k,l}e^{\bar{\jmath}2\pi\nu_{k,l}^{\mathrm{ut}}t}\delta(\tau-\tau_{k,l}^{\mathrm{ut}})\mathbf{g}_k^H, \tag{9}$$

where $\tilde{a}_{k,l}$ denotes the equivalent channel gain of the l-th path for user k after time–frequency compensation. Compared with the original channel response $\breve{\mathbf{h}}_k^H(t,\tau)$, the Doppler shift and propagation delay in the equivalent channel response $\tilde{\mathbf{h}}_k^H(t,\tau)$ have been significantly reduced. From Equation (8), the downlink equivalent channel frequency response $\mathbf{h}_k^H(t,f)$ of user k is given by

$$\mathbf{h}_k^H(t,f) = \int_{-\infty}^{\infty} \tilde{\mathbf{h}}_k^H(t,\tau)e^{-\bar{\jmath}2\pi f\tau}\mathrm{d}\tau = h_k(\tau,f)\mathbf{g}_k^H, \tag{10}$$

where $h_k(\tau,f) = \sum_{l=0}^{L_k-1}\tilde{a}_{k,l}e^{\bar{\jmath}2\pi(\nu_{k,l}^{\mathrm{ut}}t - f\tau_{k,l}^{\mathrm{ut}})}$.

The downlink frequency-domain received signal of user k over the r-th subcarrier at the s-th OFDM symbol is given by

$$y_{k,s,r} = \frac{1}{T_{\mathrm{sc}}}\int_{sT}^{sT+T_{sc}} y_{k,s}^{\mathrm{cps}}(t)e^{-\bar{\jmath}2\pi r\Delta f t}\mathrm{d}t = \mathbf{h}_{k,s,r}^H\sum_{i=1}^{K}\mathbf{b}_i x_{i,s,r} + z_{k,s,r}, \tag{11}$$

where $z_{k,s,r}$ is the AWGN noise with a mean of 0 and a variance of σ_k^2, and $\mathbf{h}_{k,s,r}^H$ denotes the downlink channel vector of user k, which can be expressed as

$$\mathbf{h}_{k,s,r}^H = \mathbf{h}_k^H(sT, r\Delta f) = h_{k,s,r}\mathbf{g}_k^H, \tag{12}$$

where $h_{k,s,r} = h_k(sT, r\Delta f)$.

For brevity, the OFDM symbol index s and subcarrier index r are omitted, and $\mathbf{h}_k = h_k\mathbf{g}_k$ is defined as the downlink channel vector of user k over a certain subcarrier. Based on the physical multipath channel model [28], h_k can be modeled using the Rician distribution, which can be expressed as

$$h_k = \sqrt{\frac{\kappa_k\beta_k}{\kappa_k+1}}h_k^{\mathrm{los}} + \sqrt{\frac{\beta_k}{\kappa_k+1}}h_k^{\mathrm{nlos}}, \tag{13}$$

where κ_k is the Rician factor, h_k^{los} denotes the line-of-sight (LOS) component of user k, h_k^{nlos} is a complex Gaussian random variable, and β_k represents the downlink average channel power of user k, i.e.,

$$\beta_k = \mathbb{E}\left\{\text{tr}(\mathbf{h}_k \mathbf{h}_k^H)\right\} = \mathbb{E}\left\{|h_k|^2\right\}. \tag{14}$$

By implementing linear precoding at the downlink transmitter and omitting the subcarrier index r and OFDM symbol index s, the downlink received signal of user k can be expressed as

$$y_k = \mathbf{h}_k^H \mathbf{B} \sum_{i=1}^{K} \sqrt{p_i} \mathbf{w}_i x_i + z_k, \tag{15}$$

where $\mathbf{B} = [\mathbf{b}_1, \cdots, \mathbf{b}_K] \in \mathbb{C}^{M \times K}$ denotes the beamforming matrix composed of K beamforming vectors; p_i is the downlink transmit power allocated to user i satisfying $\sum_i p_i \leq P_{\text{total}}$, with P_{total} being the total downlink transmit power; and $\mathbf{w}_i$ represents the downlink precoding vector for user k satisfying $||\mathbf{w}_i|| = 1$. Equation (15) can be rewritten in matrix form as

$$\mathbf{y} = \mathbf{H}^H \mathbf{B} \mathbf{W} \mathbf{P}^{1/2} \mathbf{x} + \mathbf{z}, \tag{16}$$

where $\mathbf{y} = [y_1, \cdots, y_K]^T$ is the received signal vector of the K users, $\mathbf{H} = [\mathbf{h}_1, \cdots, \mathbf{h}_K]$ represents the channel matrix between the satellite and the K users, $\mathbf{x} = [x_1, \cdots, x_K]^T$ is the downlink transmit signal vector, $\mathbf{z} = [z_1, \cdots, z_K]^T$ is the noise vector, $\mathbf{W} = [\mathbf{w}_1, \cdots, \mathbf{w}_K]$ denotes the precoding matrix for the K users, and $\mathbf{P} = \text{diag}(p_1, \cdots, p_K)$ is the power allocation matrix.

Figure 2 presents the system architecture of the downlink transmitter in a multi-beam LEO satellite communication system. First, the satellite transmitter schedules a group of users using the same time–frequency resources in each beam, and the downlink transmitter for each user generates frequency-domain transmit signals. Subsequently, the downlink precoder generates the transmit signals for each beam, and the time-domain transmit signals for each beam are formed through resource mapping and OFDM modulation. Finally, the BFN is utilized to generate transmit signals for each antenna element.

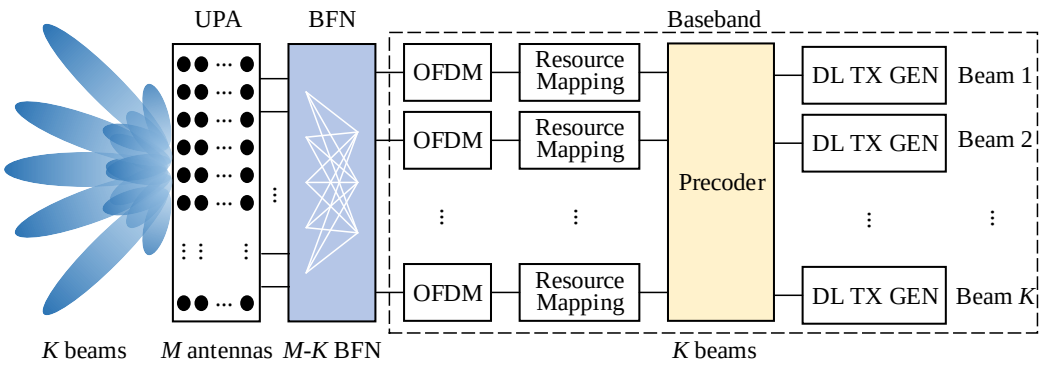


Figure 2. System architecture of satellite transmitter.

3. Conventional iCSI-Based Precoding

The ZF precoding can achieve a unit response in the desired direction and forces the response in the directions of interfering users to be zero, thereby eliminating inter-user interference (IUI), which satisfies $\mathbf{H}^H \mathbf{B} \mathbf{W} = \mathbf{I}_K$. Thus, the precoding vector of user k can be expressed as

$$\mathbf{w}_k^{\text{ZF}} = \frac{1}{\eta_k^{\text{ZF}}} (\mathbf{B}^H \mathbf{H} \mathbf{H}^H \mathbf{B})^{-1} \mathbf{B}^H \mathbf{h}_k, \tag{17}$$

where η_k^{ZF} is the normalization factor that makes $||\mathbf{w}_k^{\text{ZF}}|| = 1$.

When the channel correlation among users is high, the channel correlation matrix becomes an ill-conditioned matrix. ZF precoding will amplify noise under the condition of low signal-to-noise ratio (SNR), resulting in the degradation of system performance. To address this issue, a regularization factor is introduced into ZF precoding, and thus the RZF precoding vector for user k is given by

$$\mathbf{w}_k^{\mathrm{RZF}} = \frac{1}{\eta_k^{\mathrm{RZF}}}(\mathbf{B}^H\mathbf{H}\mathbf{H}^H\mathbf{B} + \mu\mathbf{I}_K)^{-1}\mathbf{B}^H\mathbf{h}_k, \tag{18}$$

where η_k^{RZF} is the normalization factor that makes $||\mathbf{w}_k^{\mathrm{RZF}}|| = 1$.

The MMSE precoding aims to design a precoding matrix $\mathbf{W}$ that minimizes the mean square error (MSE) between the transmitted signals $\mathbf{x}$ and the received signals $\mathbf{y}$ for all users. The MMSE precoding vector for user k can be expressed as

$$\mathbf{w}_k^{\mathrm{MMSE}} = \frac{1}{\eta_k^{\mathrm{MMSE}}}(\mathbf{B}^H\mathbf{H}\mathbf{H}^H\mathbf{B} + \frac{K\sigma_{\mathrm{n}}^2}{P_{\mathrm{total}}}\mathbf{I}_K)^{-1}\mathbf{B}^H\mathbf{h}_k, \tag{19}$$

where η_k^{MMSE} is the normalization factor that makes $||\mathbf{w}_k^{\mathrm{MMSE}}|| = 1$.

It can be observed from the aforementioned precoding vector expressions that the transmitter needs to obtain the iCSI of all users in advance when designing precoding. However, in LEO satellite communication systems, it is extremely difficult for the transmitter to acquire iCSI due to channel characteristics such as large propagation delay, Doppler shift, and high dynamic characteristics [21].

In LEO satellite mobile communication systems, the round-trip transmission delay induced by long propagation distances typically ranges from several milliseconds to over ten milliseconds. For ground user terminals moving at high speeds, the typical channel coherence time is only several milliseconds. Therefore, whether for time division duplexing (TDD) or frequency division duplexing (FDD) systems, there exists the problem of iCSI obsolescence caused by long propagation delays.

Specifically, in TDD systems, the estimated results of uplink CSI are directly used for downlink transmission. When the downlink signal arrives at the user, the previously estimated uplink CSI may have become outdated. Even if the large Doppler effect caused by satellite motion is compensated, considering only the Doppler shift generated by terminal movement, the typical channel coherence time in high-speed motion scenarios is several milliseconds. In contrast, the round-trip transmission time in satellite scenarios often ranges from several milliseconds to more than ten milliseconds, which exceeds the channel coherence time and leads to the obsolescence of the acquired iCSI. In FDD systems, each user first estimates the downlink CSI and then feeds it back to the satellite, resulting in significant overhead for channel estimation and feedback. Similarly, when the feedback-downlink CSI arrives at the satellite, it will also become outdated because the satellite–ground transmission time exceeds the channel coherence time. Therefore, the large transmission delay in satellite communication systems causes the obsolescence of iCSI, and the overhead of frequent channel feedback is also unbearable.

4. sCSI-Based Precoding Design

Compared with iCSI, sCSI can remain stable for a relatively longer period and is easier to obtain on the satellite side. Therefore, designing downlink precoding based on sCSI is more suitable for LEO satellite communication systems. In this section, we propose to design downlink precoding using sCSI and derive closed-form solutions for statistical-ZF, statistical-RZF, and statistical-MMSE precoding.

4.1. Statistical-ZF Precoder

The statistical-ZF precoding aims to eliminate the statistically averaged inter-user interference, which sets the expectation of interference power to 0 and the expectation of the corresponding user's power to 1. Therefore, we define the objective function $\mathcal{J}_{\mathrm{ZF}}(\mathbf{W})$ as

$$\mathcal{J}_{\mathrm{ZF}}(\mathbf{W}) = \mathbb{E}\left\{||\mathbf{H}^H\mathbf{B}\mathbf{W} - \mathbf{I}_K||_F^2\right\}. \tag{20}$$

The design of statistical-ZF precoding can be formulated as a minimization problem for the objective function $\mathcal{J}_{\mathrm{ZF}}(\mathbf{W})$, which is expressed as

$$\begin{aligned} &\mathcal{P}1 : \min_{\mathbf{W}} \mathcal{J}_{\mathrm{ZF}}(\mathbf{W}) \\ &\mathrm{s}.t. \mathbf{W} = [\mathbf{w}_1, \cdots, \mathbf{w}_K], \mathbf{w}_k^H\mathbf{w}_k = 1, \end{aligned} \tag{21}$$

Equation (20) can be expanded into the following form:

$$\mathcal{J}_{\mathrm{ZF}}(\mathbf{W}) = \mathbb{E}\left\{||[\mathbf{H}^H\mathbf{B}\mathbf{w}_1 - \mathbf{e}_1, \cdots, \mathbf{H}^H\mathbf{B}\mathbf{w}_K - \mathbf{e}_K]||_F^2\right\}. \tag{22}$$

where $\mathbf{e}_k$ is a column vector with the k-th element being 1 and the remaining elements being 0. Therefore, by leveraging the properties of the matrix Frobenius norm, problem $\mathcal{P}1$ can be transformed into the following problem:

$$\begin{aligned} &\mathcal{P}2 : \min_{\mathbf{w}_k} \mathcal{J}_{\mathrm{ZF}}(\mathbf{w}_k) \\ &\mathrm{s}.t. \mathbf{w}_k^H\mathbf{w}_k = 1, \end{aligned} \tag{23}$$

where $\mathcal{J}_{\mathrm{ZF}}(\mathbf{w}_k)$ is defined as

$$\mathcal{J}_{\mathrm{ZF}}(\mathbf{w}_k) = \mathbb{E}\left\{||\mathbf{H}^H\mathbf{B}\mathbf{w}_k - \mathbf{e}_k||_F^2\right\}, \tag{24}$$

Theorem 1. *The closed-form solution to the statistical-ZF precoding vector satisfying $\mathcal{P}2$ is given by*

$$\mathbf{w}_k^{S\text{-}ZF} = \frac{1}{\eta_k^{S\text{-}ZF}} \left(\sum_{i=0}^{K} \beta_i \mathbf{B}^H\mathbf{g}_i\mathbf{g}_i^H\mathbf{B}\right)^{-1} \mathbf{B}^H\mathbf{g}_k, \tag{25}$$

where $\eta_k^{S\text{-}ZF}$ is the normalization factor that makes $||\mathbf{w}_k^{S\text{-}ZF}|| = 1$.

Proof of Theorem 1. Expanding Equation (24) yields

$$\begin{aligned} \mathcal{J}_{\mathrm{ZF}}(\mathbf{w}_k) &= \mathbb{E}((\mathbf{H}^H\mathbf{B}\mathbf{w}_k - \mathbf{e}_k)^H(\mathbf{H}^H\mathbf{B}\mathbf{w}_k - \mathbf{e}_k)) \\ &= \mathbb{E}(\mathbf{w}_k^H\mathbf{B}^H\mathbf{H}\mathbf{H}^H\mathbf{B}\mathbf{w}_k - \mathbf{e}_k^H\mathbf{H}^H\mathbf{B}\mathbf{w}_k - \mathbf{w}_k^H\mathbf{B}^H\mathbf{H}\mathbf{e}_k + \mathbf{e}_k^H\mathbf{e}_k) \\ &= \mathbb{E}(\mathbf{w}_k^H\mathbf{B}^H\mathbf{H}\mathbf{H}^H\mathbf{B}\mathbf{w}_k) - \mathbb{E}(\mathbf{h}_k^H\mathbf{B}\mathbf{w}_k) - \mathbb{E}(\mathbf{w}_k^H\mathbf{B}^H\mathbf{h}_k) + 1. \end{aligned} \tag{26}$$

The expectation of each component in Equation (26) can be expressed as

$$\mathbb{E}(\mathbf{w}_k^H\mathbf{B}^H\mathbf{H}\mathbf{H}^H\mathbf{B}\mathbf{w}_k) = \mathbf{w}_k^H\mathbf{B}^H\mathbf{R}_{\mathbf{H}}\mathbf{B}\mathbf{w}_k, \tag{27a}$$

$$\mathbb{E}(\mathbf{h}_k^H\mathbf{B}\mathbf{w}_k) = \bar{h}_k\mathbf{g}_k^H\mathbf{B}\mathbf{w}_k, \tag{27b}$$

$$\mathbb{E}(\mathbf{w}_k^H\mathbf{B}^H\mathbf{h}_k) = \mathbf{w}_k^H\mathbf{B}^H\bar{h}_k\mathbf{g}_k, \tag{27c}$$

where $\mathbf{R}_{\mathbf{H}} = \mathbb{E}(\mathbf{H}\mathbf{H}^H) = \mathbb{E}\left(\sum_{k=1}^{K} \mathbf{h}_k\mathbf{h}_k^H\right) = \sum_{k=1}^{K} \beta_k\mathbf{g}_k\mathbf{g}_k^H$, and $\bar{\mathbf{h}}_k = \mathbb{E}(\mathbf{h}_k) = \bar{h}_k\mathbf{g}_k$, $\bar{h}_k = \mathbb{E}(h_k) = \sqrt{\kappa_k\beta_k/(\kappa_k+1)}|\bar{h}_k^{\mathrm{los}}|$. Here, the phase of $\bar{h}_k$ is neglected because sCSI remains invariant and is used to design the precoding vector, which will be used for signal weighting

over a relatively long time period during which the instantaneous channel response varies. Then, $\mathcal{J}_{\mathrm{ZF}}(\mathbf{w}_k)$ can be derived as

$$\mathcal{J}_{\mathrm{ZF}}(\mathbf{w}_k) = \mathbf{w}_k^H \mathbf{B}^H \mathbf{R_H} \mathbf{B} \mathbf{w}_k - \bar{h}_k \mathbf{g}_k^H \mathbf{B} \mathbf{w}_k - \mathbf{w}_k^H \mathbf{B}^H \bar{h}_k \mathbf{g}_k + 1. \tag{28}$$

As $\mathcal{J}_{\mathrm{ZF}}(\mathbf{w}_k) \geq 0$, the statistical-ZF precoding makes the expectation of inter-user interference zero, i.e., $\mathcal{J}_{\mathrm{ZF}}(\mathbf{w}_k)$ takes the minimum value of 0. Therefore, the solution to problem $\mathcal{P}2$ can be obtained by setting the conjugate gradient of $\mathcal{J}_{\mathrm{ZF}}(\mathbf{w}_k)$ with respect to $\mathbf{w}_k$ to zero. Since $\mathbf{B}^H \mathbf{R_H} \mathbf{B}$ in Equation (28) is a Hermitian matrix, we take the derivative of $\mathcal{J}_{\mathrm{ZF}}(\mathbf{w}_k)$ with respect to $\mathbf{w}_k^H$, and obtain

$$\frac{\partial \mathcal{J}_{\mathrm{ZF}}(\mathbf{w}_k)}{\partial \mathbf{w}_k^H} = \mathbf{B}^H \mathbf{R_H} \mathbf{B} \mathbf{w}_k - \mathbf{B}^H \bar{h}_k \mathbf{g}_k. \tag{29}$$

By setting $\frac{\partial \mathcal{J}_{\mathrm{ZF}}(\mathbf{w}_k)}{\partial \mathbf{w}_k^H} = 0$, the statistical-ZF precoding vector for user k can be derived as

$$\mathbf{w}_k^{\text{S-ZF}} = \frac{1}{\eta_k^{\text{S-ZF}}} \left(\sum_{i=0}^{K} \beta_i \mathbf{B}^H \mathbf{g}_i \mathbf{g}_i^H \mathbf{B} \right)^{-1} \mathbf{B}^H \mathbf{g}_k, \tag{30}$$

This completes the proof. □

4.2. Statistical-RZF Precoder

When the distance between users is relatively small, the correlation of the array response vectors increases significantly, and the correlation matrix will become ill-conditioned, leading to the degradation of system performance. To address this issue, a regularization factor is introduced into the statistical-ZF precoding in Equation (30), and thus the statistical-RZF precoding is expressed as

$$\mathbf{w}_k^{\text{S-RZF}} = \frac{1}{\eta_k^{\text{S-RZF}}} \left(\sum_{i=0}^{K} \beta_i \mathbf{B}^H \mathbf{g}_i \mathbf{g}_i^H \mathbf{B} + \mu \mathbf{I}_K \right)^{-1} \mathbf{B}^H \mathbf{g}_k, \tag{31}$$

where $\eta_k^{\text{S-RZF}}$ is the normalization factor that makes $||\mathbf{w}_k^{\text{S-RZF}}|| = 1$. When $\mu = 0$, the statistical-RZF precoding degenerates into the statistical-ZF precoding.

4.3. Statistical-MMSE Precoder

MMSE precoding aims to design a precoding matrix that minimizes the MSE between the transmitted signals and received signals of all users, while the goal of statistical-MMSE precoding is the minimization of the average MSE. Therefore, the design of statistical-MMSE precoding can be transformed into the following problem:

$$\begin{aligned} &\mathcal{P}3 : \min_{\mathbf{W}} \mathcal{J}_{\mathrm{MMSE}}(\mathbf{W}) \\ &\text{s.t. } \mathbf{w}_k^H \mathbf{w}_k = 1, \\ &\quad \mathrm{tr}(\mathbf{W}\mathbf{P}^{1/2}) \leq P_{\text{total}}, \end{aligned} \tag{32}$$

where

$$\mathcal{J}_{\mathrm{MMSE}}(\mathbf{W}) = \mathbb{E}\{\mathrm{MSE}\}, \tag{33}$$

$$\mathrm{MSE} = \mathrm{tr}\big(\mathbb{E}(\boldsymbol{\varepsilon}\boldsymbol{\varepsilon}^H)\big) = \mathrm{tr}\big(\mathbb{E}((\mathbf{x}-\mathbf{y})(\mathbf{x}-\mathbf{y})^H)\big). \tag{34}$$

Theorem 2. *The closed-form solution to the statistical-MMSE precoding vector satisfying $\mathcal{P}3$ is given by*

$$\mathbf{w}_k^{S\text{-}MMSE} = \frac{1}{\eta_k^{S\text{-}MMSE}} \left(\sum_{i=0}^{K} \beta_i \mathbf{B}^H \mathbf{g}_i \mathbf{g}_i^H \mathbf{B} + \frac{K\sigma_n^2}{P_{total}} \mathbf{I}_K \right)^{-1} \mathbf{B}^H \mathbf{g}_k, \tag{35}$$

where $\eta_k^{S\text{-}MMSE}$ is the normalization factor that makes $||\mathbf{w}_k^{S\text{-}MMSE}|| = 1$.

Proof of Theorem 2. By substituting Equation (16) into Equation (34) and defining $\mathbf{A} = \mathbf{W}\mathbf{P}^{1/2}$, we obtain $\boldsymbol{\varepsilon} = \mathbf{x} - \mathbf{H}^H\mathbf{B}\mathbf{A}\mathbf{x} - \mathbf{z}$. Assuming that all users have the same noise variance, denoted as σ_{n}^2, it follows that $\mathbb{E}(\mathbf{z}\mathbf{z}^H) = \sigma_{\mathrm{n}}^2\mathbf{I}_K$, $\mathbb{E}(\mathbf{x}\mathbf{x}^H) = \mathbf{I}_K$, and $\mathbb{E}(\mathbf{x}\mathbf{z}^H) = \mathbb{E}(\mathbf{z}\mathbf{x}^H) = \mathbf{0}$. Thus,

$$\begin{aligned} \mathbb{E}(\boldsymbol{\varepsilon}\boldsymbol{\varepsilon}^H) &= \mathbb{E}((\mathbf{x} - \mathbf{H}^H\mathbf{B}\mathbf{A}\mathbf{x} - \mathbf{z})(\mathbf{x} - \mathbf{H}^H\mathbf{B}\mathbf{A}\mathbf{x} - \mathbf{z})^H) \\ &= \mathbb{E}((\mathbf{I}_K - \mathbf{H}^H\mathbf{B}\mathbf{A})\mathbf{x}\mathbf{x}^H(\mathbf{I}_K - \mathbf{H}^H\mathbf{B}\mathbf{A})^H - (\mathbf{I}_K - \mathbf{H}^H\mathbf{B}\mathbf{A})\mathbf{x}\mathbf{z}^H \\ &\quad - \mathbf{z}\mathbf{x}^H(\mathbf{I}_K - \mathbf{H}^H\mathbf{B}\mathbf{A}) + \mathbf{z}\mathbf{z}^H) \\ &= (\mathbf{I}_K - \mathbf{H}^H\mathbf{B}\mathbf{A})(\mathbf{I}_K - \mathbf{H}^H\mathbf{B}\mathbf{A})^H + \sigma_{\mathrm{n}}^2\mathbf{I}_K. \end{aligned} \tag{36}$$

Since $\mathbb{E}(\mathrm{tr}(\mathbf{X})) = \mathrm{tr}(\mathbb{E}(\mathbf{X}))$ and $\mathrm{tr}(\mathbf{X}\mathbf{Y}) = \mathrm{tr}(\mathbf{Y}\mathbf{X})$, $\mathcal{J}_{\mathrm{MMSE}}(\mathbf{A})$ can be rewritten as

$$\begin{aligned} \mathcal{J}_{\mathrm{MMSE}}(\mathbf{A}) &= \mathrm{tr}\Big(\mathbb{E}\Big((\mathbf{I}_K - \mathbf{H}^H\mathbf{B}\mathbf{A})(\mathbf{I}_K - \mathbf{H}^H\mathbf{B}\mathbf{A})^H + \sigma_{\mathrm{n}}^2\mathbf{I}_K\Big)\Big) \\ &= (1 + \sigma_{\mathrm{n}}^2)K - 2\,\mathrm{Re}\{\mathrm{tr}(\mathbb{E}(\mathbf{H}^H)\mathbf{B}\mathbf{A})\} + \mathrm{tr}(\mathbf{A}^H\mathbf{B}^H\mathbb{E}(\mathbf{H}\mathbf{H}^H)\mathbf{B}\mathbf{A}). \end{aligned} \tag{37}$$

where $\mathbb{E}(\mathbf{H}\mathbf{H}^H) = \mathbf{R}_{\mathbf{H}}$, $\mathbb{E}\{\mathbf{H}\} = \boldsymbol{\Lambda}\mathbf{G}$, $\boldsymbol{\Lambda} = \mathrm{diag}\{\bar{h}_1, \cdots, \bar{h}_K\} \in \mathbb{C}^{K\times K}$, and $\mathbf{G} = [\mathbf{g}_1, \cdots, \mathbf{g}_K] \in \mathbb{C}^{K\times K}$.

Define the Lagrangian function as

$$\mathcal{L}(\mathbf{A}, \gamma) = \mathcal{J}_{\mathrm{MMSE}}(\mathbf{A}) + \gamma(\mathrm{tr}(\mathbf{A}\mathbf{A}^H) - P_{\mathrm{total}}), \tag{38}$$

where γ is referred to as the Lagrange multiplier. Taking the complex gradient of $\mathcal{L}(\mathbf{A}, \gamma)$ with respect to $\mathbf{A}^*$, we can obtain [29,30]

$$\frac{\partial \mathcal{L}}{\partial \mathbf{A}^*} = -\mathbf{B}^H\boldsymbol{\Lambda}\mathbf{G} + \mathbf{B}^H\mathbf{R}_{\mathbf{H}}\mathbf{B}\mathbf{A} + \gamma\mathbf{A}. \tag{39}$$

By setting $\frac{\partial \mathcal{L}}{\partial \mathbf{A}^*} = 0$, the expression for $\mathbf{A}$ can be derived as

$$\mathbf{A} = (\mathbf{B}^H\mathbf{R}_{\mathbf{H}}\mathbf{B} + \gamma\mathbf{I}_K)^{-1}\mathbf{B}^H\boldsymbol{\Lambda}\mathbf{G}. \tag{40}$$

As $\mathbf{A} = \mathbf{W}\mathbf{P}^{1/2}$, then

$$\mathbf{W} = (\mathbf{B}^H\mathbf{R}_{\mathbf{H}}\mathbf{B} + \gamma\mathbf{I}_K)^{-1}\mathbf{B}^H\mathbf{G}\boldsymbol{\Lambda}\mathbf{P}^{-1/2}. \tag{41}$$

In MMSE precoding, the parameter γ is typically set to $\gamma = K\sigma_{\mathrm{n}}^2/P_{\mathrm{total}}$. Meanwhile, by normalizing Equation (41) column-wise, the statistical-MMSE precoding vector of use k is obtained as

$$\mathbf{w}_k^{\text{S-MMSE}} = \frac{1}{\eta_k^{\text{S-MMSE}}} \left(\sum_{i=0}^{K} \beta_i \mathbf{B}^H \mathbf{g}_i \mathbf{g}_i^H \mathbf{B} + \frac{K\sigma_{\mathrm{n}}^2}{P_{\mathrm{total}}} \mathbf{I}_K \right)^{-1} \mathbf{B}^H \mathbf{g}_k. \tag{42}$$

This completes the proof. □

The statistical-ZF derivation is proven to be the optimal solution for eliminating inter-user interference in the statistical sense by minimizing the residual interference power. The

statistical-RZF derivation integrates a regularization term into the theoretical framework of statistical ZF. This fully demonstrates that the precoder achieves a balanced trade-off between interference suppression and noise amplification, thereby realizing suboptimal sum-rate performance for the system while ensuring numerical stability. The statistical-MMSE derivation is based on the minimum average MSE criterion. The derived precoding matrix is proven to be the optimal solution for minimizing the mean square error between the transmitted and received signals in the average sense, which also confirms that this precoder yields the best performance among the three proposed schemes.

Based on the aforementioned sCSI-based precoding design, the satellite downlink precoding algorithm is presented in Algorithm 1. The total computational complexity of the proposed sCSI-based precoding scheme in this paper is $MK^2 + 2K^3 + \mathcal{O}(K^3)$, where $\mathcal{O}(K^3)$ is the computational complexity of the matrix inversion. It should be noted that the sCSI-based precoding vector can be calculated within a relatively long sCSI update interval (e.g., 100 ms), which reduces the computational requirements for the satellite payload.

Algorithm 1 sCSI-based precoding

Input: $\mathbf{g}_i$ and β_i of each user, beamforming matrix $\mathbf{B}$, total transmit power P_{total}, user number K.
Output: $\mathbf{w}_k$ of each user.
1: Calculate $\mathbf{V} = \sum_{i=0}^{K} \beta_i \mathbf{B}^H \mathbf{g}_i \mathbf{g}_i^H \mathbf{B}$.
2: Calculate $\mathbf{\Gamma}$, where
$\mathbf{\Gamma} = \mathbf{V}^{-1}\mathbf{B}^H$ for statistical-ZF precoding;
$\mathbf{\Gamma} = (\mathbf{V} + \mu \mathbf{I}_K)^{-1}\mathbf{B}^H$ for statistical-RZF precoding;
$\mathbf{\Gamma} = \left(\mathbf{V} + \frac{K\sigma_n^2}{P_{\text{total}}}\mathbf{I}_K\right)^{-1}\mathbf{B}^H$ for statistical-MMSE precoding.
3: For $k = 1 : K$
4: Calculate $\mathbf{w}_k^{\text{tmp}} = \mathbf{\Gamma}\mathbf{g}_k$.
5: Calculate the normalization factor $\eta_k^{\text{tmp}} = ||\mathbf{w}_k^{\text{tmp}}||$.
6: Calculate $\mathbf{w}_k = \frac{1}{\eta_k^{\text{tmp}}}\mathbf{w}_k^{\text{tmp}}$.
7: end

5. sCSI Acquisition

According to the precoding vector expressions based on sCSI in Section 4, the required sCSI information only includes the array response vector $\mathbf{g}_k$ on the satellite side and the downlink channel average power β_k of each user. In LEO satellite communication systems, the array response vector and channel average power are closely related to the position information of the satellite and users. Based on the position information reported by users, the difficulty in acquiring sCSI can be significantly reduced.

For the array response vector $\mathbf{g}_k$, the satellite calculates the angles $(\theta_k^{\text{x}}, \theta_k^{\text{y}})$ of each user relative to the x-axis and y-axis of the satellite array antenna based on information such as the position of the scheduled user, satellite position, and satellite attitude. Then, the direction cosines $(\tilde{\theta}_k^{\text{x}}, \tilde{\theta}_k^{\text{y}})$ can be calculated according to Equation (3), and $\mathbf{g}_k$ is further calculated according to Equations (2) and (4).

For the average channel power β_k, the satellite can obtain it through downlink channel estimation and feedback from each user. However, this will increase the overhead of channel estimation and system feedback. This paper proposes an approximation method based on link gain, which is given by

$$\tilde{\beta}_k = \frac{\lambda^2 M G_k^{\text{sat}} G_k^{\text{ut}}}{(4\pi)^2 d_k^2}, \tag{43}$$

where G_k^{sat} denotes the radiation gain of the antenna element on the satellite side, which is related to the antenna pattern and the angle $(\theta_k^{\text{x}}, \theta_k^{\text{y}})$ of user k relative to the satellite antenna; G_k^{ut} represents the gain of the user receive antenna, which can be reported to the satellite along with position information; and d_k is the distance between the satellite and user k, which can be calculated using the positions of the satellite and the user. Therefore, the sCSI-based precoding method can obtain the sCSI parameters through computation, eliminating the need for users to feed back any CSI. Consequently, the system overhead associated with channel estimation and feedback is significantly reduced. The sCSI acquisition algorithm is summarized as Algorithm 2.

Algorithm 2 sCSI acquisition

Input: the coordinates and receive antenna gain G_k^{ut} of each user, the satellite coordinates, the satellite antenna gain G_k^{sat}, the satellite antenna number M, and the wavelength λ.
Output: $\mathbf{g}_i$ and β_i of each user.
1: For $k = 1 : K$
2: Calculate the angles $(\theta_k^{\text{x}}, \theta_k^{\text{y}})$ and d_k by the coordinates of user k and the satellite.
3: Calculate the direction cosines $(\tilde{\theta}_k^{\text{x}}, \tilde{\theta}_k^{\text{y}})$ according to Equation (3).
4: Calculate $\mathbf{g}_k$ according to Equations (2) and (4).
5: Calculate $\tilde{\beta}_k$ according to Equation (43).
6: end

In addition, for satellite constellations, the elevated satellite density at high latitudes gives rise to an expanded inter-satellite coverage overlap region. To alleviate inter-satellite interference, satellites are designed to deactivate partial beams and reduce their coverage scales adaptively. From the user perspective, this leads to more frequent satellite handover events, which in turn affect the acquisition and update processes of sCSI. To tackle this challenge, each satellite is able to periodically send the user location data within its current service coverage to neighboring satellites through inter-satellite links. The subsequent serving satellites can thereby pre-acquire the user positions, compute the sCSI for these users accordingly, and thus reduce the adverse performance impacts induced by satellite handovers.

6. Simulation Results

This section presents simulation results to verify the performance of the proposed downlink precoding based on sCSI. The simulation parameters are shown in Table 2. The satellite is equipped with a UPA, with an antenna spacing of half a wavelength and array sizes of 16×16, 20×20, 24×24, and 32×32, respectively. Each user employs a single antenna. The transmit gain of each antenna element on the satellite side is 6 dB, and the receive gain of the user's antenna is 0 dB. The satellite transmit power is 5–30 dBW. The number of users is 32, 64, and 96, respectively. The downlink carrier frequency is 2 GHz, the system bandwidth is 10 MHz, the subcarrier spacing is 15 kHz, and the fast Fourier transform (FFT) length is 1024. The 3GPP NTN channel model is adopted [31], where parameters such as the multipath number, path loss, shadow fading, and Rician factor are calculated according to the simulation scenario, with the first path being the LOS path. The noise variance of the user is $\sigma_k^2 = k_{\text{B}} T_{\text{n}} B_{\text{W}}$, where k_{B} is the Boltzmann constant, T_{n} is the noise temperature, and B_{W} is the downlink system bandwidth. The downlink beamforming vector adopts the discrete Fourier transform (DFT) codebook based on user positions. Monte Carlo simulations are employed to verify the performance of the proposed method. The simulation results are obtained by averaging over 1000 independent Monte Carlo trials, and the initial random seed value is fixed to 100. The performance is evaluated

under the dense urban scenario. We evaluate the system performance using the downlink ergodic sum rate, which is defined as

$$\mathcal{R}^{\text{sum}} = \sum_{k=1}^{K} \mathbb{E}\left\{ \log\left(1 + \frac{|\mathbf{h}_k^H \mathbf{B}\mathbf{w}_k|^2 p_k}{\sum\limits_{i=1, i\neq k}^{K} |\mathbf{h}_k^H \mathbf{B}\mathbf{w}_i|^2 p_i + \sigma_k^2}\right)\right\}. \tag{44}$$

Table 2. Simulation parameters.

Parameter	Value
Radius of Earth	6378 km
Orbit altitude of satellite	500 km
Orbital inclination	55°
Number of orbital planes	60
Number of satellites per orbital plane	60
Minimum user elevation	30°
Carrier frequency f_c	2 GHz
System bandwidth B_W	10 MHz
Subcarrier spacing Δf	15 KHz
FFT length N_{sc}	1024
Number of antennas at satellite $M_x \times M_y$	16×16, 20×20, 24×24, 32×32
Antenna spacing d_x, d_y	0.5λ
Satellite TX power P_{total}	5–30 dBW
Number of downlink beams K	32, 64, 96
Antenna gain G^{sat}, G_k^{ut}	6 dBi, 0 dBi
Noise temperature at the user	290 K
Beamforming vector	DFT
Simulation scenario	Dense Urban

Poisson disk sampling is adopted to generate the spatial angles of users within the satellite coverage area [28,32]. Let $\vartheta_{\max}$ denote the maximum nadir angle of the satellite; then, the nadir angle of each user satisfies $\cos\vartheta_k = \sin\theta_k^x \sin\theta_k^y = \sqrt{1 - (\tilde{\theta}_k^y)^2 - (\tilde{\theta}_k^x)^2} \geq \cos\vartheta_{\max}$, i.e., the spatial angle satisfies $(\tilde{\theta}_k^x)^2 + (\tilde{\theta}_k^x)^2 \leq \sin^2\vartheta_{\max}$. Figure 3 presents two user distribution cases with different minimum distances between users: Figure 3a shows a user distribution case with the minimum distance of the users being $\rho_{\min} = 0.035$, while Figure 3b depicts a user distribution case with the minimum distance of the users being $\rho_{\min} = 0.015$. In the figures, the black line represents the edge of the satellite coverage area, the red star denotes the spatial angle of the satellite, and the blue dots represent the spatial angles of the users.

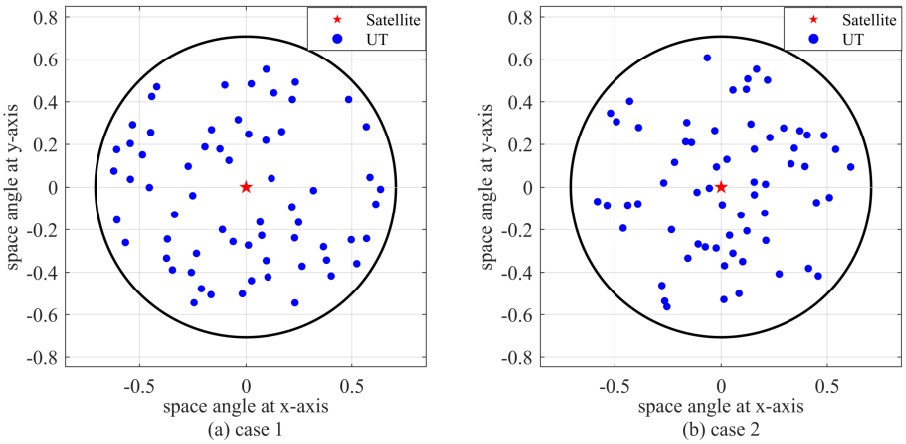


Figure 3. The satellite coverage and the distributions of users' spatial angles.

Figure 4 illustrates the downlink sum rate performance of the precoding schemes based on iCSI and sCSI under user distribution Case 1. In the figure,

- "ZF" denotes the ZF precoding based on iCSI;
- "SZF" represents the proposed statistical-ZF (SZF) precoding based on sCSI;
- "RZF" stands for the RZF precoding based on iCSI;
- "SRZF" denotes the proposed statistical-RZF (SRZF) precoding based on sCSI;
- "MMSE" indicates the MMSE precoding based on iCSI;
- "SMMSE" represents the proposed statistical-MMSE (SMMSE) precoding based on sCSI.
- "MaxSumRate" represents the precoding method proposed in [28], which maximizes the sum rate based on iCSI.

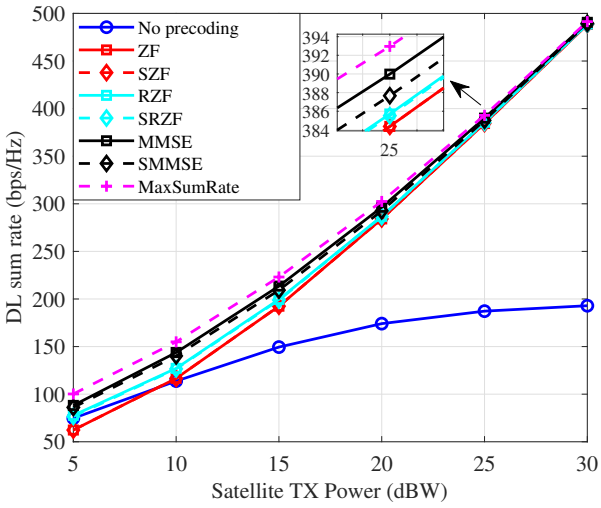


Figure 4. Comparison of the downlink sum rate performance of the precoding based on iCSI and sCSI under user distribution Case 1.

It can be observed that compared with the transmission without precoding, multi-beam precoding can significantly improve the downlink transmission performance. When the satellite transmit power is 25 dBW, the sum rate gain reaches 106%. Furthermore, the performance of the proposed sCSI-based precoding can approach that of iCSI-based precoding with negligible performance loss, and it can also approximate the optimal transmission performance of sum-rate maximization achieved by iCSI-based methods. Specifically, when the satellite transmit power is 25 dBW, the performance of statistical-MMSE based on sCSI can achieve 99.5% of that of the iCSI-based MMSE precoding, while the performance losses of statistical-RZF and statistical-ZF are only 0.05% (i.e., achieving 99.95% of the iCSI-based counterparts). In addition, when the transmit power is low, the downlink SNR is small and noise dominates, resulting in the inferior performance of ZF precoding compared with RZF and MMSE precoding. As the transmit power increases, the downlink SNR improves, and the performance of ZF precoding gradually approaches that of RZF and MMSE precoding, with the performance curves of different methods eventually converging. A detailed comparison of the above schemes is presented in Table 3.

Figure 5 presents the performance comparison of the proposed method with different power allocation strategies under user distribution Case 1. As shown in the results, the optimal transmission performance based on sum-rate maximization with iCSI outperforms all other counterparts. It is worth noting that in the precoding design oriented toward sum-rate maximization, the transmit power assigned to different users is tailored to their channel conditions. In contrast, an equal power allocation strategy across users will lead to a noticeable degradation in the system sum-rate performance. Nevertheless, the

adoption of a waterfilling-based power allocation scheme enables the proposed method to achieve enhanced sum-rate performance, thus bringing it closer to the optimal transmission performance of sum-rate maximization.

Table 3. Performance comparison of different precoding schemes under user distribution Case 1.

Method	CSI Requirements	Complexity	Sum-Rate Gains at 25 dBW
MaxSumRate	iCSI	extremely high	110.16%
ZF	iCSI	high	105.47%
RZF	iCSI	high	106.26%
MMSE	iCSI	high	108.55%
SZF	sCSI	low	105.47%
SRZF	sCSI	low	106.15%
SMMSE	sCSI	low	107.30%
No precoding	none	none	0%

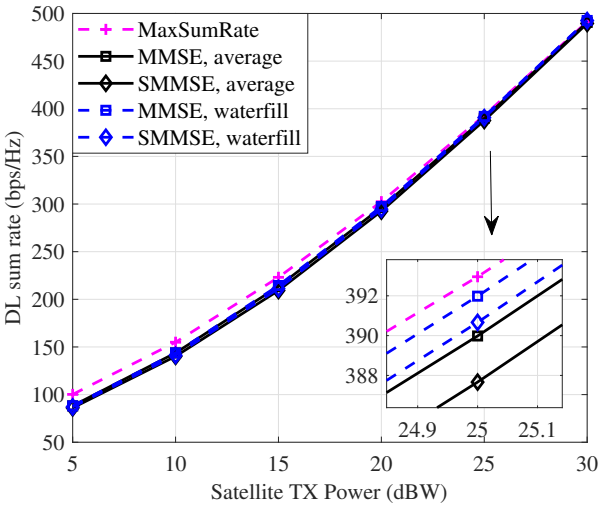


Figure 5. Comparison of the downlink sum rate performance of the precoding with different power-allocation strategies under user distribution Case 1.

Figure 6 shows the received signal-to-interference-plus-noise ratio (SINR) of different users under user distribution Case 1. We can see that compared with the transmission scheme without precoding, the received SINR can be significantly improved by adopting the multi-beam precoding method.

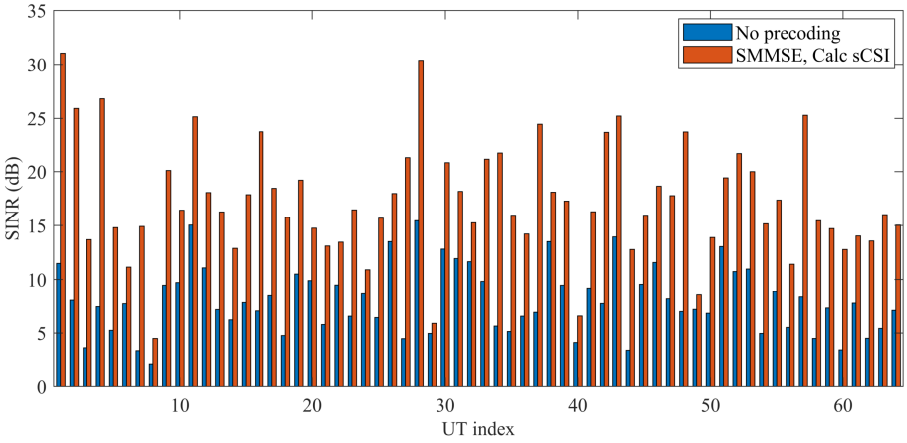


Figure 6. The received SINR of different users under user distribution Case 1.

Figure 7 presents the downlink sum rate performance of the precoding schemes based on iCSI, accurate sCSI, and calculated sCSI, adopting the RZF and MMSE criteria under

user distribution Case 1, respectively. Compared with the transmission performance based on accurate sCSI, the transmission performance of the proposed sCSI calculated from position information incurs an extremely small and almost negligible loss. Specifically, when the satellite transmit power is 25 dBW, the performance loss of the statistical-RZF precoding based on the calculated sCSI is only 0.08%, while that of the statistical-MMSE precoding based on the calculated sCSI is merely 1.70%.

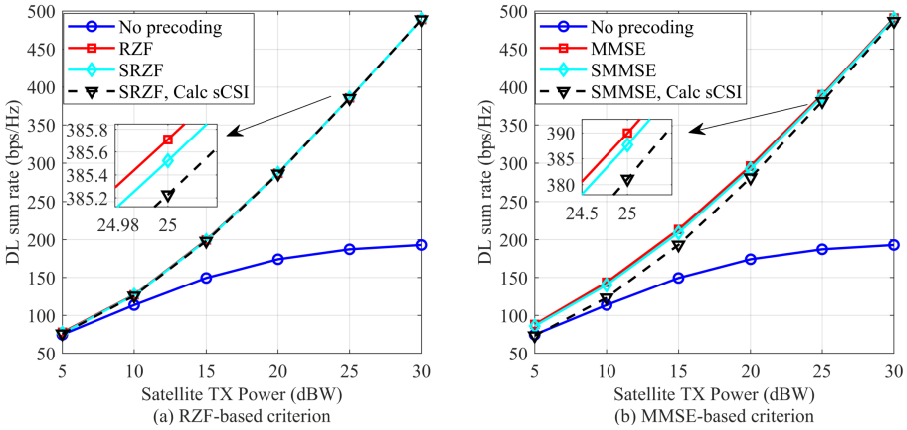


Figure 7. Comparison of the downlink sum rate performance of the precoding based on iCSI, accurate sCSI, and calculated sCSI under user distribution Case 1.

Figure 8 shows the impact of different beam pointing deviations (BPDs) on the transmission performance of the proposed precoding under user distribution Case 1. The large-scale PAAs are widely adopted in LEO communication satellites. However, after the satellite is in orbit, various non-ideal factors, such as satellite orbital errors, attitude errors, coordinate calculation accuracy, beam calculation errors, array installation accuracy, and array deformation caused by thermodynamic factors, lead to deviations in the actual beam pointing, thereby resulting in a degradation of system performance [33,34]. It can be observed from the figure that the proposed method exhibits better robustness against BPD. Specifically, when the satellite transmit power is 25 dBW, the performance losses caused by 0.1° and 0.2° BPD are only 1.13% and 3.86%, respectively, for statistical-RZF precoding, while the performance losses induced by 0.1° and 0.2° BPD are merely 0.75% and 2.95%, respectively, for statistical-MMSE precoding.

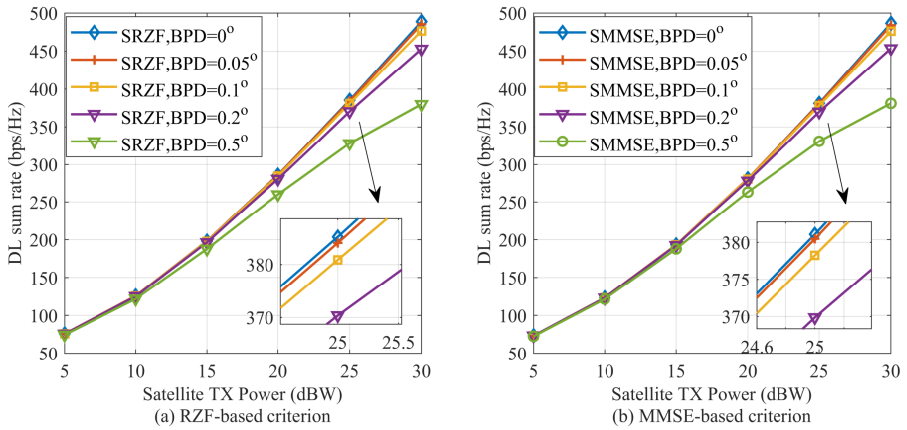


Figure 8. Comparison of the downlink sum rate performance under different BPDs under user distribution Case 1.

Figure 9 illustrates the impact of different sCSI update periods on the precoding performance under user distribution Case 1. It can be observed that even with an up-

date period of 200 ms, the downlink sum rate performance loss is extremely small, even negligible. Specifically, when the satellite transmit power is 25 dBW, the performance losses of statistical-RZF and statistical-MMSE precoding with a 200 ms update period are 2.41% and 2.12%, respectively. This indicates that the calculation of precoding vectors can be completed within a relatively long sCSI update period, reducing the computational complexity of on-board payload processing.

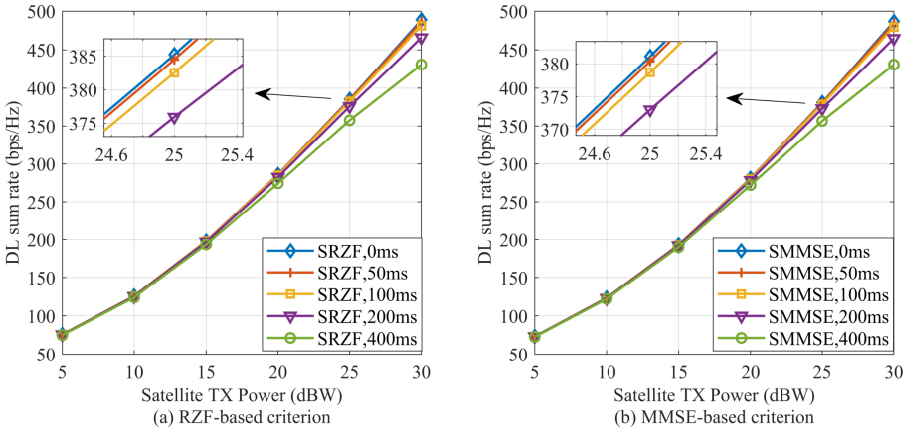


Figure 9. Comparison of the downlink sum rate performance under different sCSI update periods under user distribution Case 1.

Figure 10 illustrates the downlink sum rate performance of the precoding methods based on iCSI and sCSI under user distribution Case 2, in which the minimum distance between users is reduced, and some users have close spatial angles, resulting in increased inter-user interference. It can be observed from the simulation results that compared with the transmission method without precoding, multi-beam precoding can significantly improve the system sum rate performance. The sum rate of the statistical MMSE precoder is improved by 115%. The performance of the proposed sCSI-based precoding can approach that of the iCSI-based precoding with a small performance loss. Specifically, when the satellite transmit power is 25 dBW, the performance of statistical-MMSE based on sCSI can achieve 96.9% of that of the iCSI-based MMSE precoding, while the performance loss of statistical-RZF is only 0.07%. In addition, when the transmit power is low, the downlink SNR is small and noise dominates, resulting in the inferior performance of ZF precoding compared with RZF and MMSE precoding. Furthermore, compared with Figure 4, the minimum distance between users in user distribution Case 2 is smaller, which means that the inter-user interference is increased. In this case, the system sum-rate performance is lower than that in user distribution Case 1. As can be seen from the comparative simulation results of the two cases, the better the user scheduling (i.e., the lower the inter-user interference), the better the system sum-rate performance achieved by precoding transmission. Meanwhile, the performance gap between sCSI-based precoding and iCSI-based precoding becomes narrower.

Figure 11 presents the performance comparison of the proposed method with different power allocation strategies under user distribution Case 2. The sum-rate performance of statistical MMSE precoding with equal power allocation reaches 93.31% of the optimal transmission performance based on sum-rate maximization precoding. However, when the water-filling power allocation scheme is adopted, the performance of statistical MMSE precoding can reach 96.79% of this optimal transmission performance.

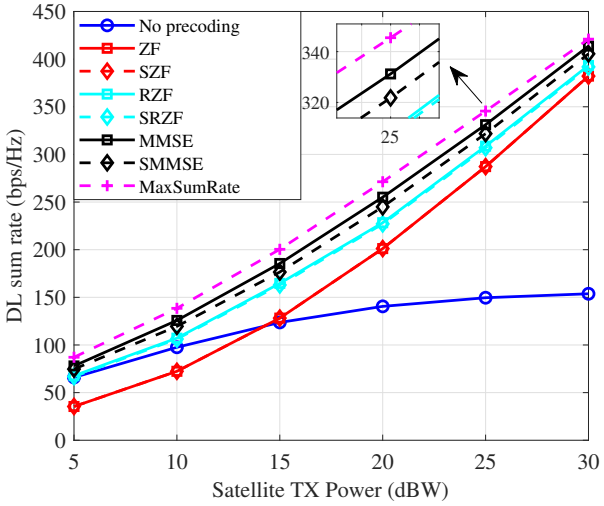


Figure 10. Comparison of the downlink sum rate performance of the precoding based on iCSI and sCSI under user distribution Case 2.

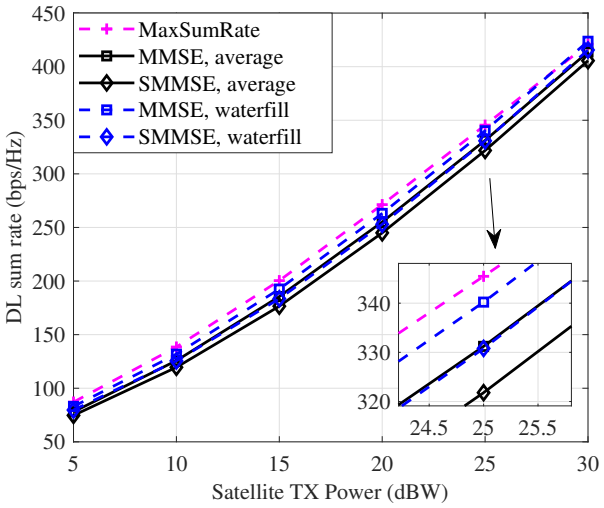


Figure 11. Comparison of the downlink sum rate performance of the precoding with different power-allocation strategies under user distribution Case 2.

Figure 12 shows the received SINR of different users under user distribution Case 2. In this case, the minimum distance between users decreases, which leads to a sharp increase in interference among some users and a subsequent drop in the received SINR. However, the adoption of the multi-beam precoding method results in a significant improvement in the received SINR of users.

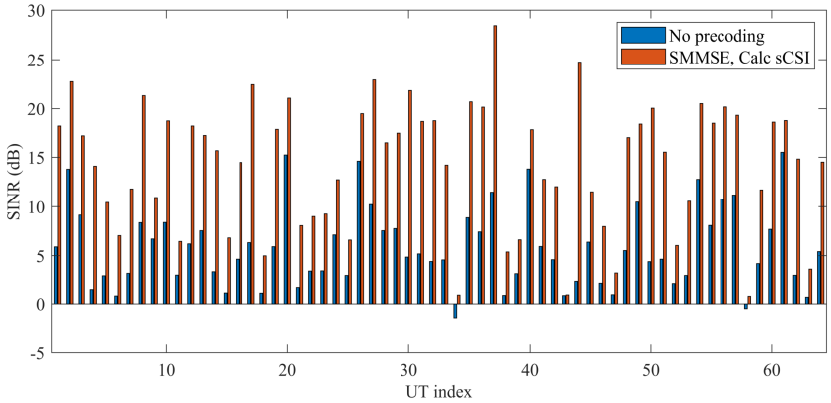


Figure 12. The received SINR of different users under user distribution Case 2.

Figure 13 presents the downlink sum rate performance of the precoding schemes based on iCSI, accurate sCSI, and calculated sCSI, adopting the RZF and MMSE criteria under user distribution Case 2, respectively. Compared with the transmission performance based on accurate sCSI, the transmission performance of the proposed sCSI calculated from position information incurs an extremely small and almost negligible loss. Specifically, when the satellite transmit power is 25 dBW, the performance loss of the statistical-RZF precoding based on the calculated sCSI is only 0.62%, while that of the statistical-MMSE precoding based on the calculated sCSI is merely 3.16%.

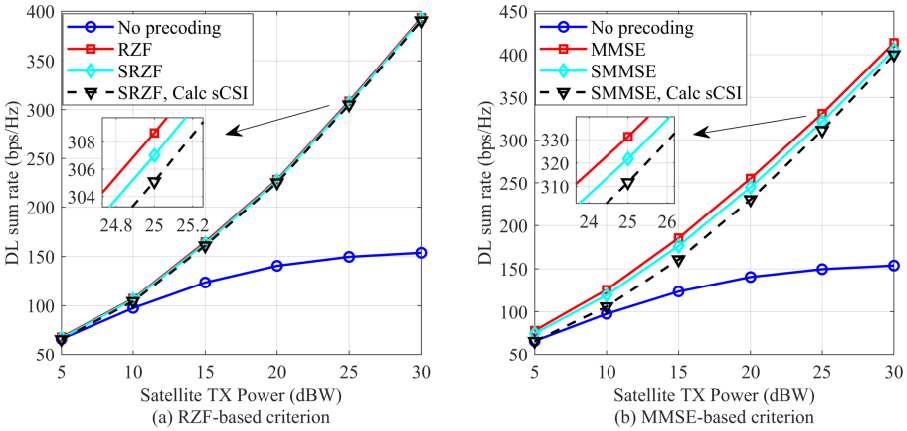


Figure 13. Comparison of the downlink sum rate performance of the precoding based on iCSI, accurate sCSI, and calculated sCSI under user distribution Case 2.

Figure 14 shows the impact of different BPDs on the transmission performance of the proposed precoding under user distribution Case 2. It can be observed from the figure that the proposed method still exhibits excellent robustness against various BPD values. Specifically, when the satellite transmit power is 25 dBW, the performance loss caused by a BPD of even 0.2° is extremely small.

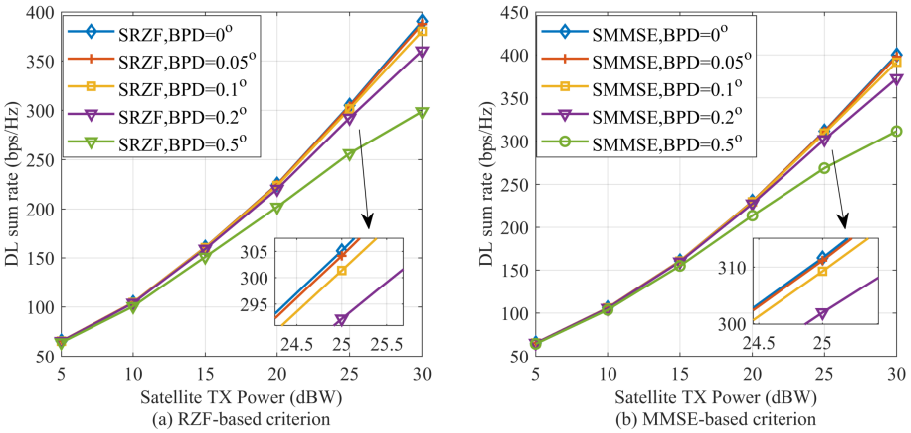


Figure 14. Comparison of the downlink sum rate performance under different BPD under user distribution Case 2.

Figure 15 illustrates the impact of different sCSI update periods on the precoding performance under user distribution Case 2. Similarly, even with an update period of 200 ms, the downlink sum rate performance loss is extremely small, even negligible. Specifically, when the satellite transmit power is 25 dBW, the performance losses of statistical-RZF and statistical-MMSE precoding with a 200 ms update period are 2.62% and 2.57%, respectively.

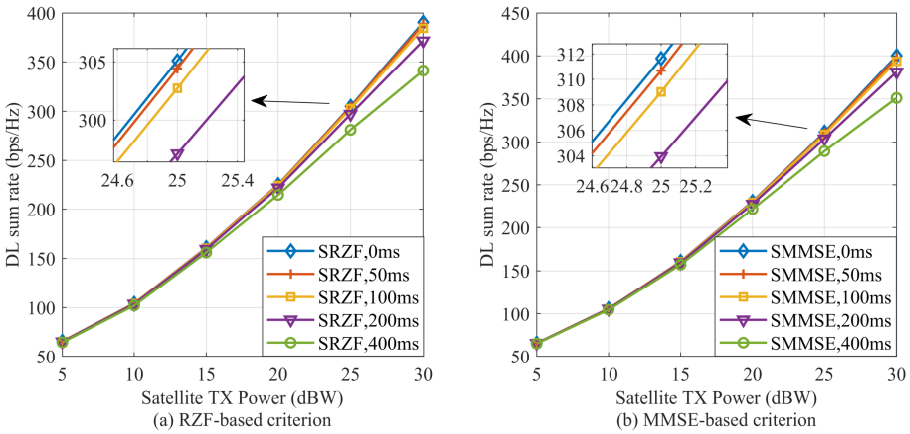


Figure 15. Comparison of the downlink sum rate performance under different sCSI update periods under user distribution Case 2.

Figure 16 presents the comparison of downlink sum rate performance under different numbers of users and beams for user distribution Case 1, where the satellite is equipped with a 20 × 20 UPA. It can be observed that the system downlink sum-rate performance improves as the number of users increases. However, as the number of users further increases, the inter-user interference rises accordingly, and the performance gap of the sCSI-based precoding method also widens. Despite this trend, the performance of the proposed sCSI-based precoding can approach both the optimal transmission performance derived from sum-rate maximization and the performance of iCSI-based precoding, which verifies the superiority of the proposed method under varying user numbers.

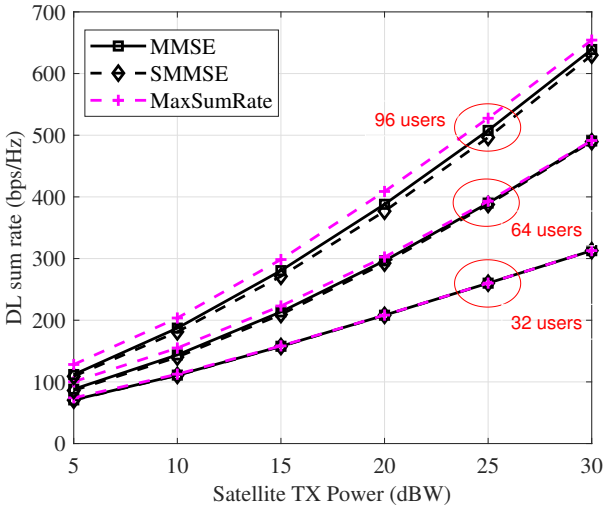


Figure 16. Downlink sum rate performance comparison under different user/beam numbers.

Figure 17 illustrates the sum-rate performance comparison when the satellite is equipped with different antenna numbers. As the number of antennas increases, the antenna array gain increases, and the system sum-rate performance is improved accordingly. Moreover, a larger number of antennas enables more refined beams, which reduces inter-user interference and narrows the performance gap of the proposed method. It is demonstrated that the proposed sCSI-based precoding method can approach both the optimal transmission performance and the iCSI-based precoding performance across all tested antenna number configurations.

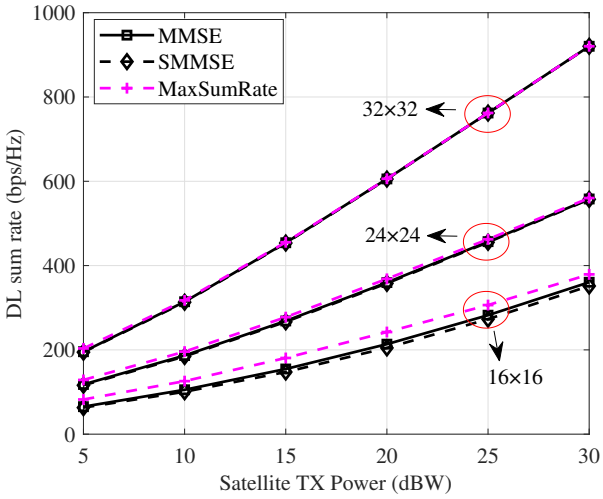


Figure 17. Downlink sum rate performance comparison under different antenna numbers.

7. Conclusions

In this paper, we investigate the downlink precoding design for multi-beam LEO satellite communication systems based on sCSI. First, we establish the downlink channel and signal transmission models for OFDM-based LEO satellite communication systems. Then, we propose to design downlink precoding using sCSI and derive closed-form solutions for statistical-ZF, statistical-RZF, and statistical-MMSE precoding. The required sCSI only includes the array response vectors of each user on the satellite side and the average downlink channel power, which are closely related to the position information of the satellite and users. Compared with iCSI, sCSI is substantially easier to acquire at the transmitter. Precoding vectors based on sCSI can be computed over a longer sCSI update period, reducing the computational requirements for on-board processing. Subsequently, we propose a method to calculate sCSI using information such as satellite position and user position. Thus, users only need to periodically report their position information without estimating and feeding back CSI, which significantly reduces system overhead. Ultimately, we present numerical simulation results to demonstrate that the proposed method can substantially improve the system sum-rate performance. Notably, the proposed method requires users to obtain their own coordinates, which are generally accessible via the global navigation satellite system (GNSS). However, GNSS outages or interference will either hinder users from acquiring coordinate information or degrade positioning accuracy. Future work will focus on developing more robust user positioning methods to eliminate reliance on GNSS. In addition, the proposed sCSI-based precoding framework can be extended to hybrid analog–digital architectures. Specifically, the joint optimization of analog beamforming vectors and statistical digital precoding vectors can be investigated, considering constraints such as limited RF chains, phase shifter quantization errors, and on-board equipment power consumption. Furthermore, the sCSI-based precoding method can be extended to multi-satellite scenarios, which will substantially reduce inter-satellite information exchange.

Author Contributions: Conceptualization, F.Z.; methodology, F.Z.; software, F.Z. and Y.W.; validation, F.Z., Y.W., and Z.X.; formal analysis, Y.W. and Z.X.; investigation, F.Z.; data curation, F.Z.; writing—original draft preparation, F.Z.; writing—review and editing, X.G.; visualization, F.Z. and Y.W.; supervision, X.G.; project administration, F.Z. and X.G.; funding acquisition, X.G. All authors have read and agreed to the published version of the manuscript.

Funding: This work was supported by the Jiangsu Province Major Science and Technology Project under Grant BG2024005, the Fundamental Research Funds for the Central Universities under Grant 2242022k60007, the Key R&D Plan of Jiangsu Province under Grant BE2022067, the Civil Aerospace Technology Pre-research Project under Grant D030301.

Data Availability Statement: The original contributions of this study are presented in this article, and further inquiries can be directed towards the corresponding author.

Conflicts of Interest: The authors declare no conflicts of interest.

Abbreviations

The following abbreviations are used in this manuscript:

3GPP	the 3rd-generation partnership
5G	5th generation
6G	6th generation
AoD	angles of departure
AWGN	additive white Gaussian noise
BFN	beamforming network
CP	cyclic prefix
CSI	channel state information
DFT	discrete Fourier transform
DTD	direct-to-device
FDD	frequency division duplex
FFR	full frequency reuse
FFT	fast Fourier transform
GEO	geostationary earth orbit
HTS	high throughput satellite
ITU	international telecommunication union
iCSI	instantaneous channel state information
IUI	inter-user interference
LEO	low Earth orbit
LOS	line-of-sight
MIMO	multiple-input multiple-output
MMSE	minimum mean square error
MSE	mean square error
OFDM	orthogonal frequency division multiplexing
PAA	phased array antenna
NR	new radio
NTN	non-terrestrial networks
RZF	regularized zero-forcing
sCSI	statistical channel state information
SINR	signal-to-interference-plus-noise ratio
SNR	signal-to-noise ratio
TDD	time division duplex
UPA	uniform planar array
ZF	zero-forcing

References

1. Giordani, M.; Zorzi, M. Non-Terrestrial Networks in the 6G Era: Challenges and Opportunities. *IEEE Netw.* **2021**, *35*, 244–251. [CrossRef]
2. Kodheli, O.; Lagunas, E.; Maturo, N.; Sharma, S.K.; Shankar, B.; Mendoza Montoya, J.F. Satellite Communications in the New Space Era: A Survey and Future Challenges. *IEEE Commun. Surv. Tutor.* **2021**, *23*, 70–109. [CrossRef]
3. Zhu, X.; Jiang, C. Integrated Satellite-Terrestrial Networks Toward 6G: Architectures, Applications, and Challenges. *IEEE Internet Things J.* **2022**, *9*, 437–461. [CrossRef]

4. Liu, R.; Zhang, L.; Li, R.Y.-N.; Renzo, M.D. The ITU Vision and Framework for 6G: Scenarios, Capabilities, and Enablers. *IEEE Veh. Technol. Mag.* **2025**, *20*, 114–122. [CrossRef]
5. Liu, R.; Lin, H.; Lee, H.; Chaves, F.; Lim, H.; Sköld, J. Beginning of the Journey Toward 6G: Vision and Framework. *IEEE Commun. Mag.* **2023**, *61*, 8–9. [CrossRef]
6. Boumard, S.; Moilanen, I.; Lasanen, M.; Suihko, T.; Höyhtyä, M.A. Technical Comparison of Six Satellite Systems: Suitability for Direct-to-Device Satellite Access. In Proceedings of the 2023 IEEE 9th World Forum on Internet of Things (WF-IoT), Aveiro, Portugal, 12–27 October 2023; pp. 1–6.
7. Taha, H.; Vári, P.; Lapsánszky, A. Direct-to-Device Satellite Communications in the European Union: Spectrum Allocation and Regulatory Pathways Within the ITU Framework. *IEEE Access* **2025**, *13*, 190556–190581. [CrossRef]
8. Pasandi, H.B.; Fraire, J.A.; Ratnasamy, S.; Rivano, H. A Survey on Direct-to-Device Satellite Communications: Advances, Challenges, and Prospects. In Proceedings of the 2nd International Workshop on LEO Networking and Communication (LEO-NET '24), Washington, DC, USA, 18 November 2024; Association for Computing Machinery: New York, NY, USA, 2024; pp. 7–12.
9. Guidotti, A.; Vanelli-Coralli, A. Geographical Scheduling for Multicast Precoding in Multi-Beam Satellite Systems. In Proceedings of the 2018 9th Advanced Satellite Multimedia Systems Conference and the 15th Signal Processing for Space Communications Workshop (ASMS/SPSC), Berlin, Germany, 10–12 September 2018; IEEE: Piscataway, NJ, USA, 2018; pp. 1–8.
10. Rinaldi, F.; Määttänen, H.-L.; Torsner, J.; Pizzi, S.; Andreev, S.; Iera, A. Broadcasting Services Over 5G NR Enabled Multi-Beam Non-Terrestrial Networks. *IEEE Trans. Broadcast.* **2021**, *67*, 33–45. [CrossRef]
11. 3GPP. Proposal Title: Vision for NTN in 6G. In Proceedings of the 3GPP TSG RAN 6G Workshop, Incheon, Republic of Korea, 10–11 March 2025; Proposal No. 6GWS-250027.
12. 3GPP. Proposal Title: Space for 6G and Sustainable Connectivity. In Proceedings of the 3GPP TSG RAN 6G Workshop, Incheon, Republic of Korea, 10–11 March 2025; Proposal No. 6GWS-250169.
13. 3GPP. Proposal Title: NTN Related Views on 6G RAN WG SI. In Proceedings of the 3GPP TSG RAN#108, Prague, Czech Republic, 9–13 June 2025; Proposal No. RP-251001.
14. 3GPP. Proposal Title: Views on 6G for NTN and Aerospace Networks. In Proceedings of the 3GPP TSG RAN#108, Prague, Czech Republic, 9–13 June 2025; Proposal No. RP-251358.
15. Zheng, G.; Chatzinotas, S.; Ottersten, B. Generic Optimization of Linear Precoding in Multibeam Satellite Systems. *IEEE Trans. Wirel. Commun.* **2012**, *11*, 2308–2320. [CrossRef]
16. Chien, T.V.; Lagunas, E.; Ta, T.H.; Chatzinotas, S.; Ottersten, B. User Scheduling and Power Allocation for Precoded Multi-Beam High Throughput Satellite Systems with Individual Quality of Service Constraints. *IEEE Trans. Veh. Technol.* **2023**, *72*, 907–923. [CrossRef]
17. Chen, L.; Ha, V.N.; Lagunas, E.; Wu, L.; Chatzinotas, S.; Ottersten, B. The Next Generation of Beam Hopping Satellite Systems: Dynamic Beam Illumination with Selective Precoding. *IEEE Trans. Wirel. Commun.* **2023**, *22*, 2666–2682. [CrossRef]
18. Han, Z.; Yang, T.; Liu, R. On Beam Hopping Pattern Design for Satellite Communication Systems with Hybrid Precoding. *IEEE Trans. Veh. Technol.* **2024**, *73*, 1364–1369. [CrossRef]
19. Wang, J.; Qi, C.; Yu, S. Hybrid Beamforming Design for Beam-Hopping LEO Satellite Communications. In Proceedings of the GLOBECOM 2023—2023 IEEE Global Communications Conference, Kuala Lumpur, Malaysia, 4–8 December 2023; pp. 3959–3964.
20. Yuan, S.; Sun, Y.; Peng, M.; Yuan, R. Joint Beam Direction Control and Radio Resource Allocation in Dynamic Multi-Beam LEO Satellite Networks. *IEEE Trans. Veh. Technol.* **2024**, *73*, 8222–8237. [CrossRef]
21. You, L.; Li, K.-X.; Wang, J.; Gao, X.Q.; Xia, X.-G.; Ottersten, B. Massive MIMO Transmission for LEO Satellite Communications. *IEEE J. Sel. Areas Commun.* **2020**, *38*, 1851–1865. [CrossRef]
22. You, L.; Liu, A.; Wang, W.; Gao, X. Outage Constrained Robust Multigroup Multicast Beamforming for Multi-Beam Satellite Communication Systems. *IEEE Wirel. Commun. Lett.* **2019**, *8*, 352–355. [CrossRef]
23. Wang, W.; Liu, A.; Zhang, Q.; You, L.; Gao, X.; Zheng, G. Robust Multigroup Multicast Transmission for Frame-Based Multi-Beam Satellite Systems. *IEEE Access* **2018**, *6*, 46074–46083. [CrossRef]
24. Wang, W.; Liu, A.; You, L.; Gao, X.; Zheng, G.; Chatzinotas, S. Resource Efficiency Optimization for Robust Beamforming in Multi-Beam Satellite Communications. *IEEE Trans. Veh. Technol.* **2021**, *70*, 6958–6968. [CrossRef]
25. Ahmad, I.; Nguyen, K.D.; Letzepis, N.; Lechner, G.; Joroughi, V. Zero-Forcing Precoding With Partial CSI in Multibeam High Throughput Satellite Systems. *IEEE Trans. Veh. Technol.* **2021**, *70*, 1410–1420. [CrossRef]
26. Ashraf, S.; Saleem, S.; Ahmed, T.; Arfeen, Z.A. Succulent Link Selection Strategy for Underwater Sensor Network. *Int. J. Comput. Sci. Math.* **2022**, *15*, 224–242. [CrossRef]
27. Schröder, A.; Gracla, S.; Röper, M.; Wübben, D.; Bockelmann, C.; Dekorsy, A. Flexible Robust Beamforming for Multibeam Satellite Downlink Using Reinforcement Learning. In Proceedings of the 2024 IEEE International Conference on Communications (ICC), Denver, CO, USA, 9–13 June 2024; IEEE: Piscataway, NJ, USA, 2024; pp. 3809–3814.

28. Li, K.-X.; You, L.; Gao, X.-G.; Ottersten, B. Downlink Transmit Design for Massive MIMO LEO Satellite Communications. *IEEE Trans. Commun.* **2022**, *70*, 1014–1028. [CrossRef]
29. Joham, M.; Utschick, W.; Nossek, J.A. Linear Transmit Processing in MIMO Communications Systems. *IEEE Trans. Signal Process.* **2005**, *53*, 2700–2712. [CrossRef]
30. Seo, B.; Shin, J. Equivalence Between SLNR and MMSE Precoding Schemes in the K-User MISO Interference Channel. *Wseas Trans. Signal Process.* **2015**, *11*, 23–28.
31. 3GPP. *Study on New Radio (NR) to Support Non-Terrestrial Networks (Release 15)*; TR 38.811, V15.1.0; 3rd Generation Partnership Project (3GPP): Sophia Antipolis, France, July 2020.
32. Bridson, R. Fast Poisson Disk Sampling in Arbitrary Dimensions. In Proceedings of the ACM SIGGRAPH 2007, San Diego, CA, USA, 5–9 August 2007; Association for Computing Machinery: New York, NY, USA, 2007; pp. 1–7.
33. Sun, C.; Jiang, H.; Zhang, J.; Tao, Y.; Li, B.; Zhao, C. Modeling and Calibrating the Ground-Surface Beam Pointing of GEO Satellite. *IEEE Access* **2019**, *7*, 121897–121906. [CrossRef]
34. Yang, L.; Li, Y.; Liu, A.; Jin, S. In Orbit Pointing Calibration Scheme and Performance Simulation of Multi-Beam Antenna. In Proceedings of the 2022 IEEE MTT-S International Wireless Symposium (IWS), Harbin, China, 12–15 August 2022; IEEE: Piscataway, NJ, USA, 2022; pp. 1–3.

Disclaimer/Publisher's Note: The statements, opinions and data contained in all publications are solely those of the individual author(s) and contributor(s) and not of MDPI and/or the editor(s). MDPI and/or the editor(s) disclaim responsibility for any injury to people or property resulting from any ideas, methods, instructions or products referred to in the content.